Influence of Implant Neck Design on Bone Formation Under Mechanical Repetitive Loading: Histomorphometric and Microcomputed Tomographic Studies in Rabbit Tibiae

Munenori Yasutake, DDS,*,# Shinichiro Kuroshima, DDS, PhD,†,# Takuya Ishimoto, PhD,††, Takayoshi Nakano, PhD,|| and Takashi Sawase, DDS, PhD§

* Postgraduate Student, Department of Applied Prosthodontics, Graduate School of Biomedical Sciences, Nagasaki University, Nagasaki, Japan.

† Assistant Professor, Department of Applied Prosthodontics, Graduate School of Biomedical Sciences, Nagasaki University, Nagasaki, Japan.

†† Assistant Professor, Division of Materials and Manufacturing Science, Graduate School of Engineering, Osaka University, Osaka, Japan.

|| Professor, Division of Materials and Manufacturing Science, Graduate School of Engineering, Osaka University, Osaka, Japan.

§ Professor, Department of Applied Prosthodontics, Graduate School of Biomedical Sciences, Nagasaki University, Nagasaki, Japan.

Reprinted requests and correspondence to : Takashi Sawase, DDS, PhD, Department of Applied Prosthodontics, Graduate School of Biomedical Sciences, Nagasaki University, 1-7-1, Sakamoto, Nagasaki, 852-8588, Japan, Phone: +81-95-819-7685, Fax: +81-95-819-7689 E-mail; sawase@nagasaki-u.ac.jp

# These authors (Munenori Yasutake and Shinichiro Kuroshima) contributed equally to this work.

All authors have no conflicts of interest

ABSTRACT

Purpose: *The aim of this study was to investigate effects of implant neck design on the original concept of osseointegration and bone formation when applying mechanical repetitive loading via bone-integrated implants.*

Materials and Methods: *Twenty-eight anodized Ti-6Al-4V alloy implants with +60° or -60° grooves in the implant neck were placed in the proximal tibial metaphysis of fourteen rabbits. Fourteen implants received mechanical repetitive loading along the long axis of the implant for 8 weeks at 12 weeks after implant placement. The remaining 14 implants received no loading. Histomorphometric and microcomputed tomographic analyses were then performed.*

Results: *No effect of neck design was observed without mechanical loading, while osseointegration around the +60° grooves was upregulated with mechanical loading. Calculated load effects on bone structure around the implant neck with +60° grooves were larger when compared with the -60° grooves under mechanical loading.*

Conclusions: *These findings indicate that the establishment of osseointegration and bone formation around the implant neck with +60° grooves is superior to those with -60° grooves under loaded conditions.*

Key words: osseointegration, bone wound healing, mechanical repetitive stimulation, oriented grooves

INTRODUCTION

Implant therapy is one of the most reliable treatment options for replacing missing teeth. After the delivery of implant-supported fixed or removable prostheses, bone-integrated implants constitutively receive mechanical repetitive loads during mastication, swallowing, and/or parafunctional movements, such as clenching and grinding via the prostheses. It is thought that the maintenance of crestal bone levels around dental implants is a critical factor for determining implant therapeutic success, although many clinical studies have reported a large number of clinical factors affecting long-term implant stability. Nonetheless, the influence of functional and/or parafunctional loading on bone around dental implants is unclear, as load quantification is challenging in both animal and clinical studies.

The term “osseointegration” was first defined as “a direct structural and functional connection between ordered living bone and the surface of a load-carrying implant”[1]. Many clinical and animal studies have reported osseointegration using newly developed implants, but most studies have been performed without mechanical loading. There have been several animal studies in which implants have been placed in dog or monkey mandibles with prostheses in order to investigate the load-bearing tolerance of bone tissue around implants[2-4]. However, there are no data on magnitude and frequency of loads applied to the prostheses and implants, although they receive bite force and transfer the load to surrounding bone tissue. Therefore, methodology to clarify the relationship between “mechanical loading” and “bone tissue around implants” is required in both animal and clinical studies.

Recently, we developed a compressor driving implant loading device that can be fixed with implants, and applied mechanical repetitive loading with variable magnitude and frequency[5]. We demonstrated that the bone tissue around implants showed anabolic responses after application of certain levels of mechanical repetitive loading using this device. In particular, bone microstructures around the implant neck varied markedly[5], thus suggesting that the neck design of dental implants plays an important role in implant stability. Moreover, several finite element analyses (FEA) have shown the highest stress to be concentrated at the coronal portion of the bone and implant interface[6, 7].

This information allowed us to devise a strategy for optimizing dental implant design in order to enhance bone quantity and contribute to implant stability, as well as long-term fixation, under loading. In the present experiment, we focused on the coronal portion of implant design, which has oriented groove architecture at the sub-hundred-micrometer level. The aims of the current study were: 1) to determine which neck designs affect bone formation around implants under non-loaded conditions, 2) to investigate bone formation with different neck designs of dental implants under loaded conditions, and 3) to clarify which neck designs effectively induce bone anabolic responses to mechanical loading.

MATERIALS AND METHODS

Implant Neck Designs

Twenty-eight anodized Ti-6Al-4V alloy dental implants were used in this study (3.7 × 6.0 mm, Kyocera Co., Ltd., Kyoto, Japan). Implants were randomly divided in two groups; “+60° grooves” and “-60° grooves” were introduced around the neck of each implant by machining (Kyocera). In the present study, “+60° grooves” and “-60° grooves” referred to the groove angles relative to a plane perpendicular to the long axis of the implant (“60° clockwise” and “60° counterclockwise” direction, respectively). Groove widths were 400 μm (Fig. 1, A).

Animals and Implant Placement

Fourteen adult female Japanese white rabbits weighing 3.8 - 4.2 kg (Biotek Co., Ltd., Saga, Japan) were used in this study. Rabbits were housed in the animal experiment facility of Nagasaki University, and fed a standard diet and water. Fifty six Ti-6Al-4V screws (Kyocera) were used for anchoring custom-made loading devices (Higuchi Co., Ltd., Nagasaki, Japan). The designed implants and two anchor screws were unicortically placed in each metaphysis of rabbit tibiae with a combination of general anesthesia (35 mg/kg ketamine and 5 mg/kg xylazine), and local anesthesia using lidocaine. Implants with +60° grooves were randomly placed in the right or left tibiae, and implants with -60° grooves

were placed on the remaining side. Next, 0.05 mg/kg buprenorphine was intramuscularly provided just after surgery, and 0.01 mg/kg buprenorphine was also provided every 12 hours for three days. Animal care and experimental procedures were performed in accordance with the Guidelines for Animal Experimentation of Nagasaki University, with approval from the Ethics Committee for Animal Research.

Load Schedules

Twelve weeks after implant placement, all implants received post abutments. Implants with -60° and +60° grooves in tibiae of seven randomly selected rabbits were subjected to mechanical repetitive loading under general anesthesia, as described previously[5] (n = 7). Briefly, implants received mechanical loading at 50 N with a frequency of 3 Hz for 1800 cycles, 2 days/week for eight weeks using the loading device supported by two lateral screws on each implant, under general anesthesia with a combination of 35 mg/kg ketamine and 5 mg/kg xylazine. Load direction was parallel to the long axis of implants. Implants in the remaining seven rabbits were not subjected to any mechanical loading (control) (n = 7) (Fig. 1, B and C).

Microcomputed Tomography (MicroCT) Assessment

All rabbits were sacrificed with an overdose of pentobarbital sodium (intravenous injection, somnopentyl; Kyoritsu Seiyaku Co., Ltd., Tokyo, Japan) at eight weeks after load onset. Tibial blocks with implants and anchor screws were dissected with a diamond saw (Exakt®; Heraeus Kulzer GmbH, Hanau, Germany). After fixation for 48 hours in 10 % formalin, microCT scans were performed at 20-μm voxel resolution with 90-kV tube voltage (R_mCT2; Rigaku Co., Ltd., Tokyo, Japan). Bone around the implants in the proximal tibial metaphysis were segmented and reconstructed using the semimanual contouring method with TRI/3D-Bon (Ratoc System Engineering, Tokyo, Japan)[8]. The regions of interest (ROIs) were the region between 50 μm and 550 μm away from the implant surface in order to avoid the metal artifacts[9], and 1800 μm below the implant neck. Extracortical bone area above the implant neck was not included in the ROI (Fig. 1, D). Digital images obtained from microCT scans were converted to

the 16-bit gray-scale TIFF format using the Atlas TIFF Converter® (Rigaku), and were observed and analyzed using TRI/3D-Bon application software. Bone volume fraction [BVF (%) = bone volume in ROI / tissue volume in ROI], the number of trabecular bone (Tb.N), the thickness of trabecular bone (Tb.Th), the distance between trabecular bones (Tb.Sp), and bone mineral density (BMD) were semi-automatically measured in accordance with the guidelines for assessment of bone microstructure using microCT[10].

Histology

Tibial bone blocks were embedded in methyl methacrylate resin (Methyl methacrylate polymer and monomer [Wako Pure Chemical Industries, Ltd., Osaka, Japan]) after dehydration with ethanol. The resin-embedded tibial blocks were cut longitudinally to include the implant and anchor screws using an Exakt® diamond saw. Specimens were ground to around 15-μm thickness. Toluidine blue stain was conducted, and histomorphometric analyses were performed in order to detect: 1) bone implant contact (BIC); 2) bone area fraction (BAF); and 3) bone thickness around the implant neck. Each area of interest (AOI) was defined as follows, 1) BIC (%) = length of bone to implant contact from implant neck to lower border of third grooves (mm) / the implant length from neck to lower border of third grooves (mm) × 100 (Fig. 1, E); 2) BAF (%) = total bone area between 0 μm and 500 μm away from the implant surface (mm^2) / total area between 0 μm and 500 μm away from implant surface (mm^2) × 100 (Fig. 1, F); and 3) bone thickness (μm) = length of bone from implant neck to lower border of newly formed bone extending downward form original cortex at 0 μm, 250 μm, 500 μm and 750 μm away from the implant surface (Fig. 1, G). Extracortical bone above the implant neck was not included in the AOI.

Statistics

Statistical analyses were conducted in a blind manner. Shapiro Wilk test was performed for normality. Paired *t* test was used for comparison between the -60° and +60° groove implants under non-

loaded conditions. Independent *t* test was performed for comparison between non-loaded and loaded conditions. Independent *t* test was also used for comparison of load effects between -60° and +60° grooves. All statistical analyses were conducted using JMPR 10 (SAS Institute Inc., Cary, NC, USA). An α-level of 0.05 was used for statistical significance. All data are given as mean ± SEM. In the present study, "load effect" was defined as the adjusted ratio under loaded conditions for each value under non-loaded conditions.

RESULTS

Effects of Implant Neck Designs on Bone Formation under Non-loaded Conditions

In order to compare effects of implant neck designs on bone formation, histomorphometric analyses were performed under non-loaded condition. All implants and screws showed good integration with bone tissue. Based on the representative images of toluidine-blue sections, bone formation around the neck was similar for the -60° and +60° groove implants (Fig. 2, A), with BIC and BAF showing similar values for both types (Fig. 2, B and C, respectively). Moreover, bone thickness around the implant neck with -60° grooves was almost the same as for that with +60° grooves, irrespective of distance from the implant surface (Fig. 2, D).

Effects of Mechanical Repetitive Loading on Bone Tissue around Implant Neck with -60° Grooves

Next, to investigate effects of mechanical loading on bone around the implant neck with -60° grooves, histomorphometric analyses and microCT scans were performed. All implants and screws showed well integrated with bone (Fig. 3, A). BIC around the neck with -60° grooves did not change, regardless of loading (Fig. 3, B). BAF and all bone thickness under loaded conditions were significantly higher when compared with non-loaded condition (Fig. 3, C and D).

From the representative microCT images, bone formation occurred downward from the implant neck under loaded conditions (Fig. 3, E). BV/TV did not change, irrespective of loading (Fig. 3, F). The number of trabecular bone (Tb.N) and the distance between each trabecular bone (Tb.Sp) did not change

between non-loaded and loaded conditions (Fig. 3, G and I, respectively), while the thickness of trabecular bone under loaded conditions was significantly higher when compared with that under non-loaded conditions (Fig. 3, H). BMD was also significantly higher in response to mechanical loading (Fig. 3, J).

Effects of Mechanical Repetitive Loading on Bone Tissue around Implant Neck with +60° Grooves

To address the impact of mechanical repetitive loading on bone around the implant neck with +60° grooves, histomorphometric analyses and microCT scans were conducted. No implants or screws showed any sign of infection (Fig. 4, A). In contrast to bone tissue around the implant neck with -60° grooves, BIC around the neck with +60° grooves under loaded condition was significantly higher when compared with that under non-loaded conditions (Fig. 4, B). BAF and bone thickness under loaded conditions were significantly higher when compared with non-loaded condition (Fig. 4, C and D).

Based on the representative microCT images, bone formation occurred downward from the implant neck under loaded conditions (Fig. 4, E). In contrast to bone around the implant neck with -60° grooves, greater BVF under loaded conditions was noted, as compared with that under non-loaded condition, but no significant differences were observed (Fig. 4, F). Tb.N was significantly higher, and Tb.Sp was lower in response to mechanical loading (Fig. 4, G and I, respectively), whereas Tb.Th did not change, regardless of loading (Fig. 4, H). BMD was significantly higher in response to mechanical loading (Fig. 4, J).

Loaded Implants with +60° Grooves Strongly Influenced Bone Structure as Compared with -60° Grooves

Finally, to investigate which implant neck designs induce more bone anabolic action in response to loading, the effects of loading on each parameter in microCT analyses were assessed based on the adjusted ratio under loaded conditions for each value under non-loaded conditions. The effects of mechanical loading on BV/TV, Tb.N and Tb.Sp around the neck with +60° grooves were significantly

larger than those with -60° grooves (Fig. 5, A, B and D). However, the effects of mechanical loading on Tb.Th and BMD were similar, regardless of implant design (Fig. 5, C and E).

DISCUSSION

This study showed that bone formation did not differ between the “+60° grooves” and “-60° grooves” under non-loaded conditions. Furthermore, this study also demonstrated that originally defined “osseointegration” and bone formation around the implant neck with +60° grooves was significantly enhanced by mechanical repetitive loading along the long axis of the implant, as compared with -60° grooves.

Marginal bone loss around dental implants, which is thought to be correlated with stress distribution during functional and/or non-functional loading, plays an important role in treatment successes and failures[11]. Even negligible forces may be transmitted to the marginal bone, resulting in bone resorption with a smooth neck, while retentive elements such as microthreads at the implant neck will dissipate forces, leading to the maintenance of crestal bone height in accordance with Wolff’s law[12]. On the other hand, the original definition of “osseointegration” is “a direct structural and functional connection between ordered living bone and the surface of a load-carrying implant”[1]. This means that mechanical loading is a prerequisite for the establishment and maintenance of “osseointegration”. Numerous studies have reported that the introduction of the effective elements in the crestal portion of the implants may contribute to the improvement of osseointegration and the maintenance of crestal bone levels in response to stress concentration occurring at the implant neck[13-16], thus suggesting that the neck design of dental implants is a crucial factor affecting osseointegration and marginal bone levels. However, the quantification of force amplitude and frequency, and load cycle number and duration have not been performed in most studies due to the difficulty in quantifying these parameters. Therefore, there is little evidence that load conditions affect the original concept of “osseointegration” and the maintenance of crestal bone around the implant neck.

In the current study, loading conditions were 50 N with a frequency of 3 Hz for 1800 cycles, 2 days/week for 8 weeks using a custom made loading device, similarly to our previous study[5]. The conditions 50 N and 3 Hz were equivalent to 1661 ± 123.65 μstrain/second (strain rate) using cadaver samples (data not shown). This value ranges from 1500 - 3000 μstrain, which promotes osteogenesis in response to mechanical stimulation according to the mechanostat theory[17]. Indeed, mechanical repetitive loading affected bone around the implant neck, irrespective of groove angle. Therefore, it is thought that the applied loading was appropriate to assess the effects of mechanical loading on "osseointegration" and bone formation around different neck designs in this study, although the selection of load cycle number and load duration are still controversial[18, 19].

Recently, we performed FEA and animal experiments using hip implants with -60°, -30°, 0°, +30° and +60° grooves. These studies demonstrated that maximum principal stress was only observed along the direction of the groove depth with +60° grooves, but not -60°, -30°, 0°, and +30° grooves[20]. From this viewpoint, we hypothesized that the neck design with +60° grooves would be more effective for bone formation in response to mechanical stresses when compared with -60° grooves. Hence, the implant neck was modified by machining +60° and +60° groove angles. On the other hand, groove width was 400 μm. Grooves with either 110 μm or 200 μm width / 70 μm depth at the thread frank showed significantly higher removal torque (approximately 30 % higher) and affinity for bone formation than control implants in rabbit tibiae and femura[21]. Moreover, it has also been reported that grooves with 110 μm width and 70 μm depth on the center of the inferior thread flank facilitate more rapid bone integration and improve implant stability[22]. These data suggest that 100 - 200 μm width / 70 μm depth at the thread may optimize bone formation and implant stability. However, some *in vitro* and *in vivo* reports have demonstrated that pore diameter >300 μm showed better osteogenesis due to accelerated osteoblast activity, much vascularization, and high oxygenation; although, the diameter did not affect cell penetration depth[23, 24]. Additionally, smaller diameters of <75 μm and 90 - 120 μm induced only fibrous tissue formation and chondrogenesis before osteogenesis, whereas larger diameters of >300 μm directly induced bone formation[24-27]. Accordingly, groove width was set at 400 μm for both +60° and -60° grooves.

The application of a custom-made loading device to intraoral placement sites was technically challenging. A previous study has reported that the bone volume in female New Zealand white rabbits is similar between tibiae and maxillae[28]. Our previous study confirmed that mechanical repetitive loading via bone-integrated implants without grooves placed in rabbit tibiae influenced the bone around dental implants[5]. Therefore, we used rabbit tibiae, instead of jaw bones in this study.

Under non-loaded conditions, bone formation around implant necks with +60° and -60° grooves was similar at 12 weeks after implant placement. In rabbit tibiae, 8 - 12 weeks are needed to reestablish normal bone structure after surgical intervention[29, 30], indicating that bone formation around dental implants under non-loaded conditions actually indicates bone wound healing until 12 weeks after implant placement. Therefore, our findings demonstrate that groove angles do not affect bone wound healing unless loading is applied via implants. Next, to evaluate the net effect of mechanical repetitive loading on bone structure and “osseointegration”, mechanical loading was applied at 12 weeks after implant placement. Interestingly, the influence of mechanical repetitive loading on bone around the implant neck differed between +60° and -60° grooves. “Osseointegration”, bone thickness, and BMD were upregulated around the implant neck with +60° grooves under loaded conditions. Moreover, a trend of more bone volume around the neck with +60° grooves was observed. On the other hand, both “osseointegration” and bone volume around the implant neck with -60° grooves did not differ between under non-loaded and loaded conditions, although bone thickness and BMD increased in response to mechanical loading. Indeed, calculated load effects on bone volume, trabecular number and trabecular separation around the implant neck with +60° grooves, were significantly larger than those with -60° grooves. These findings suggest that bone control in response to mechanical loading around the implant neck with +60° grooves was superior to that with -60° grooves. Recently, we demonstrated that increased bone formation around hip implants with +60° grooves, as compared with -60° grooves, because maximum principal stress was observed along the direction of groove depth with +60° grooves, but not with -60° grooves[20]. Our findings were consistent with this previous report; however, that study used hip implants. Hence, the developed implant designs with +60° grooves, but not -60° grooves could contribute to enhanced “osseointegration”

and the maintenance of marginal bone volume. On the other hand, calculated load effects on trabecular thickness and BMD were similar between the +60° and -60° grooves. Increased BMD with mechanical loading in the present study was in accordance with our previous study[5], and it has been demonstrated that bone cells, particularly osteocytes, play a central role in response to mechanical loading, inducing bone anabolic and/or catabolic reactions[31, 32]. Hence, animal studies focusing on cell biology are required to clarify the reasons why trabecular thickness and BMD were similar with the +60° and -60° grooves under loaded conditions.

CONCLUSIONS

Within limitations of the present study, we demonstrated that: 1) bone control was similar between the +60° and -60° grooves under non-loaded conditions; and 2) the original concept of “osseointegration” and bone formation around the implant neck with +60° grooves were superior to when compared with -60° grooves when mechanical repetitive loading along the long axis of dental implants was applied. Newly developed implant with +60° grooves around the neck, may contribute to long-term implant stability by maintaining higher rates of “osseointegration” and crestal bone levels in response to mechanical repetitive loading.

DISCLOSURE

The authors claim to have no financial interest, either directly or indirectly, in the products or information listed in this article.

ACKNOWLEDGEMENTS

This work was supported by JSPS KAKENHI Grant Numbers 22390368, 15H05030 and 15K20449.

REFERENCES:

1. Mavrogenis AF, Dimitriou R, Parvizi J, et al. Biology of implant osseointegration. *J Musculoskelet Neuronal Interact.* 2009;9:61-71.

2. Barbier L, Schepers E. Adaptive bone remodeling around oral implants under axial and nonaxial loading conditions in the dog mandible. *Int J Oral Maxillofac Implants.* 1997;12:215-223.

3. Heitz-Mayfield LJ, Schmid B, Weigel C, et al. Does excessive occlusal load affect osseointegration? An experimental study in the dog. *Clin Oral Implants Res.* 2004;15:259-268.

4. Cochran DL, Schenk RK, Lussi A, et al. Bone response to unloaded and loaded titanium implants with a sandblasted and acid-etched surface: a histometric study in the canine mandible. *J Biomed Mater Res.* 1998;40:1-11.

5. Kuroshima S, Yasutake M, Tsuiki K, et al. Structural and Qualitative Bone Remodeling Around Repetitive Loaded Implants in Rabbits. *Clin Implant Dent Relat Res.* 2015. doi:10.1111/cid.12318. [Epub ahead of print].

6. Kitamura E, Stegaroiu R, Nomura S, et al. Influence of marginal bone resorption on stress around an implant--a three-dimensional finite element analysis. *J Oral Rehabil.* 2005;32:279-286.

7. Chun HJ, Cheong SY, Han JH, et al. Evaluation of design parameters of osseointegrated dental implants using finite element analysis. *J Oral Rehabil.* 2002;29:565-574.

8. Kuroshima S, Al-Salihi Z, Yamashita J. Parathyroid hormone related to bone regeneration in grafted and nongrafted tooth extraction sockets in rats. *Implant Dent.* 2013;22:71-76.

9. Bernhardt R, Kuhlisch E, Schulz MC, et al. Comparison of bone-implant contact and bone-implant volume between 2D-histological sections and 3D-SRμCT slices. *Eur Cell Mater.* 2012;23:237-247; discussion 247-238.

10. Bouxsein ML, Boyd SK, Christiansen BA, et al. Guidelines for assessment of bone microstructure in rodents using micro-computed tomography. *J Bone Miner Res.* 2010;25:1468-1486.

11. Albrektsson T, Zarb G, Worthington P, et al. The long-term efficacy of currently used dental implants: a review and proposed criteria of success. *Int J Oral Maxillofac Implants.* 1986;1:11-25.

12. Frost HM. A 2003 update of bone physiology and Wolff's Law for clinicians. *Angle Orthod.* 2004;74:3-15.

13. Palmer RM, Palmer PJ, Smith BJ. A 5-year prospective study of Astra single tooth implants. *Clin Oral Implants Res.* 2000;11:179-182.

14. Abrahamsson I, Berglundh T. Tissue characteristics at microthreaded implants: an experimental study in dogs. *Clin Implant Dent Relat Res.* 2006;8:107-113.

15. Lee DW, Choi YS, Park KH, et al. Effect of microthread on the maintenance of marginal bone level: a 3-year prospective study. *Clin Oral Implants Res.* 2007;18:465-470.

16. Schrotenboer J, Tsao YP, Kinariwala V, Wang HL. Effect of microthreads and platform switching on crestal bone stress levels: a finite element analysis. *J Periodontol.* 2008;79:2166-2172.

17. Frost HM. Bone's mechanostat: a 2003 update. *Anat Rec A Discov Mol Cell Evol Biol.* 2003;275:1081-1101.

18. Rubin CT, Lanyon LE. Regulation of bone formation by applied dynamic loads. *J Bone Joint Surg Am.* 1984;66:397-402.

19. Kaspar D, Seidl W, Neidlinger-Wilke C, et al. Proliferation of human-derived osteoblast-like cells depends on the cycle number and frequency of uniaxial strain. *J Biomech.* 2002;35:873-880.

20. Noyama Y, Nakano T, Ishimoto T, et al. Design and optimization of the oriented groove on the hip implant surface to promote bone microstructure integrity. *Bone.* 2013;52:659-667.

21. Hall J, Miranda-Burgos P, Sennerby L. Stimulation of directed bone growth at oxidized titanium implants by macroscopic grooves: an in vivo study. *Clin Implant Dent Relat Res.* 2005;7 Suppl 1:S76-82.

22. Yoon HI, Yeo IS, Yang JH. Effect of a macroscopic groove on bone response and implant stability. *Clin Oral Implants Res.* 2010;21:1379-1385.

23. Tsuruga E, Takita H, Itoh H, et al. Pore size of porous hydroxyapatite as the cell-substratum controls BMP-induced osteogenesis. *J Biochem.* 1997;121:317-324.

24. Kuboki Y, Jin Q, Takita H. Geometry of carriers controlling phenotypic expression in BMP-induced osteogenesis and chondrogenesis. *J Bone Joint Surg Am.* 2001;83-A Suppl 1:S105-115.

25. Kuboki Y, Jin Q, Kikuchi M, et al. Geometry of artificial ECM: sizes of pores controlling phenotype expression in BMP-induced osteogenesis and chondrogenesis. *Connect Tissue Res.* 2002;43:529-534.

26. Jin QM, Takita H, Kohgo T, et al. Effects of geometry of hydroxyapatite as a cell substratum in BMP-induced ectopic bone formation. *J Biomed Mater Res.* 2000;51:491-499.

27. Hulbert SF, Young FA, Mathews RS, et al. Potential of ceramic materials as permanently implantable skeletal prostheses. *J Biomed Mater Res.* 1970;4:433-456.

28. Slotte C, Lundgren D, Sennerby L, Lundgren AK. Surgical intervention in enchondral and membranous bone: intraindividual comparisons in the rabbit. *Clin Implant Dent Relat Res* 2003; 5: 263-268

29. Breine U, Johansson B, Roylance PJ, et al. Regeneration of bone marrow. A clinical and experimetnal study following removal of bone marrow by curettage. *Acta Anat (Basel).* 1964;59:1-46.

30. Danckwardt-Lilliestrom G. Reaming of the medullary cavity and its effect on diaphyseal bone. A fluorochromic, microangiographic and histologic study on the rabbit tibia and dog femur. *Acta Orthop Scand Suppl.* 1969;128:1-153.

31. Weinbaum S, Cowin SC, Zeng Y. A model for the excitation of osteocytes by mechanical loading-induced bone fluid shear stresses. *J Biomech.* 1994;27:339-360.

32. Bellido T. Osteocyte-driven bone remodeling. *Calcif Tissue Int.* 2014;94:25-34.

FIGURE LEGENDS

Fig.1. A, Implant neck designs with +60° and -60° grooves. **B**, Itinerary in the present study. Randomly selected rabbits received mechanical loading for 8 weeks (n = 7) at 12 weeks after implant placement. The remaining rabbits received no loading (n = 7). **C**, Mechanical loading was applied to dental implants using a loading device anchored with two screws. Load conditions were 50 N, 3 Hz, and 1800 cycles twice a week for eight weeks. **D**, Regions of interest (ROIs) for microCT analysis were between 50 μm and 550 μm away from implant surface and from top of implant, to 1800 μm below the implant neck. **E**, Area of interest (AOI) for BIC. Red line indicates length of implant from implant neck to the inferior border of designated region (white dotted line shows top of implant.). **F**, AOI for BAF. Red area, which was used for measurement of bone area, was between 0 μm and 500 μm away from implant surface (white dotted line indicates top of implant.). **G**, AOIs for bone thickness. Each line indicates length of bone thickness at 250, 500, and 750 μm away from implant surface (white dotted line shows top of implant.).

Fig. 2. Bone tissues around the implant necks under non-loaded conditions; histomorphometric analyses. **A**, Representative longitudinal images of toluidine blue-stained sections (white and red dotted lines indicate top of implant and inferior border of third grooves, respectively). Bar = 500 μm. **B**-**D**, BIC, BAF and bone thicknesses around neck were similar between -60° and +60° grooves.

Fig. 3. Effects of mechanical loading on bone tissues around implant neck with -60° grooves; histomorphometric and microCT analyses. **A**, Representative longitudinal images of toluidine blue-stained sections (white and red dotted lines indicate top of implant and inferior border of grooves, respectively.) Bar = 500 μm. **B**, BIC did not change, irrespective of loading. **C** and **D**, BAF and bone thicknesses were significantly increased under loaded conditions. **E**, Representative longitudinal microCT images (white and red dotted lines indicate top of implant and inferior border of grooves, respectively.). **F**, BVF was similar, regardless of loading. **G**-**I**, Tb.N and Tb.Sp also did not change, irrespective of loading, whereas Tb.Th was significantly elevated under loaded conditions. **J**, BMD was significantly higher under

loaded conditions (n ≥ 6 per group, ** $P < 0.01$, *** $P < 0.001$).

Fig. 4. Effects of mechanical loading of bone tissues around implant neck with +60° grooves; histomorphometric and microCT analyses. **A**, Representative longitudinal images of toluidine blue-stained sections including implants with +60°grooves (white and red dotted lines indicate top of implant and inferior border of grooves, respectively.). Bar = 500 μm. **B**-**D**, BIC, BAF and bone thickness were significantly higher under loaded condition. **E**, Representative longitudinal microCT images (white and red dotted lines indicate top of implant and inferior border of grooves, respectively.). **F**, BVF under loaded conditions was elevated; however, there were no significant differences. **G**, Tb.N under loaded conditions was significantly higher than that under non-loaded condition. **H**, Tb.Sp under loaded conditions was lower, but no significant differences were observed. **I**, Tb.Th was similar, irrespective of loading. **J**, BMD was significantly higher under loaded conditions (n ≥ 6 per group, ** $P < 0.01$, *** $P < 0.001$).

Fig. 5. Effects of mechanical repetitive loading on bone microarchitecture among different implant designs. **A**, **B** and **D**, Calculated load effects on BVF, Tb N and Tb.Sp around the implant neck with +60° grooves were significantly bigger than that with -60° grooves. **B** and **E**, Calculated load effects on Tb.Th and BMD did not change around the implant neck between the -60° grooves and +60° grooves (n ≥ 6 per group, * $P < 0.05$, *** $P < 0.001$).

Fig.1

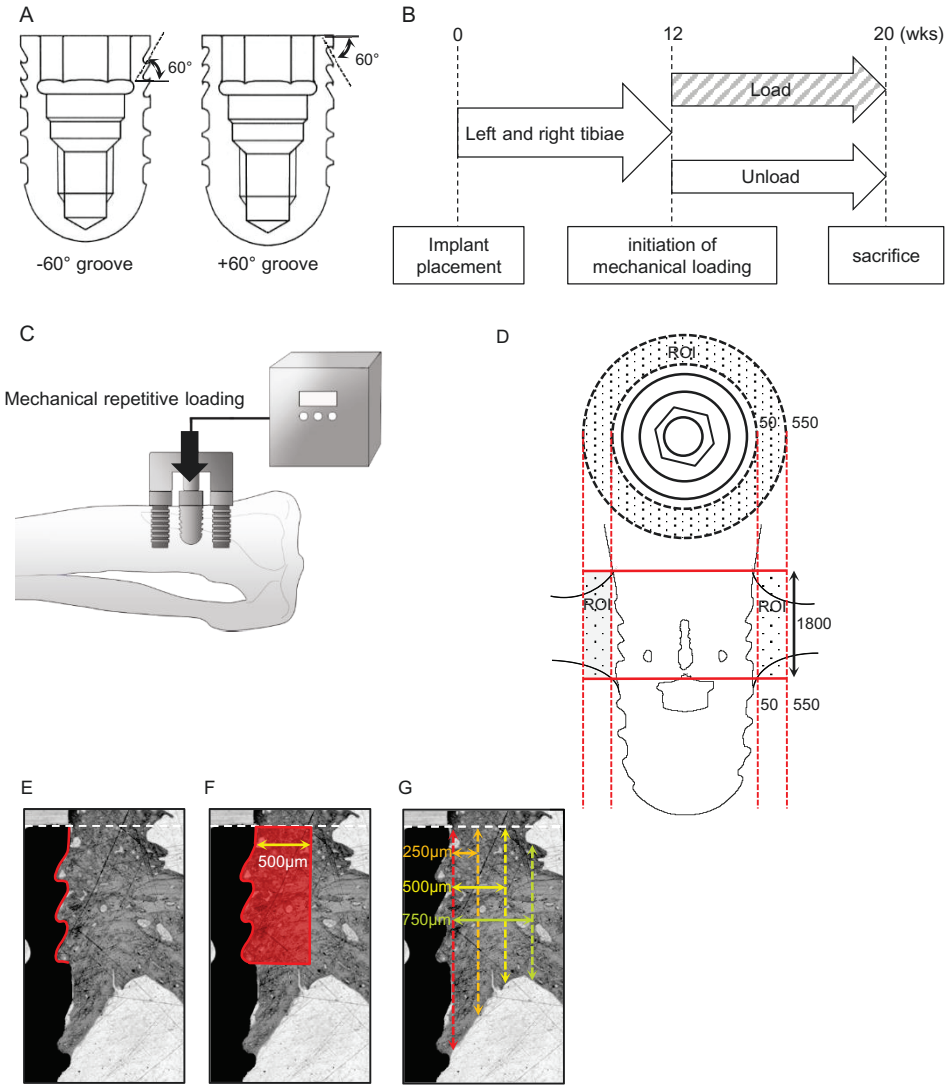
A
60°
60°
-60° groove
+60° groove
B
0
12
20 (wks)
Load
Left and right tibiae
Unload
Implant placement
initiation of mechanical loading
sacrifice
C
Mechanical repetitive loading
D
ROI
50
550
ROI
ROI
1800
50
550
E
F
500μm
G
250μm
500μm
750μm

Fig. 2

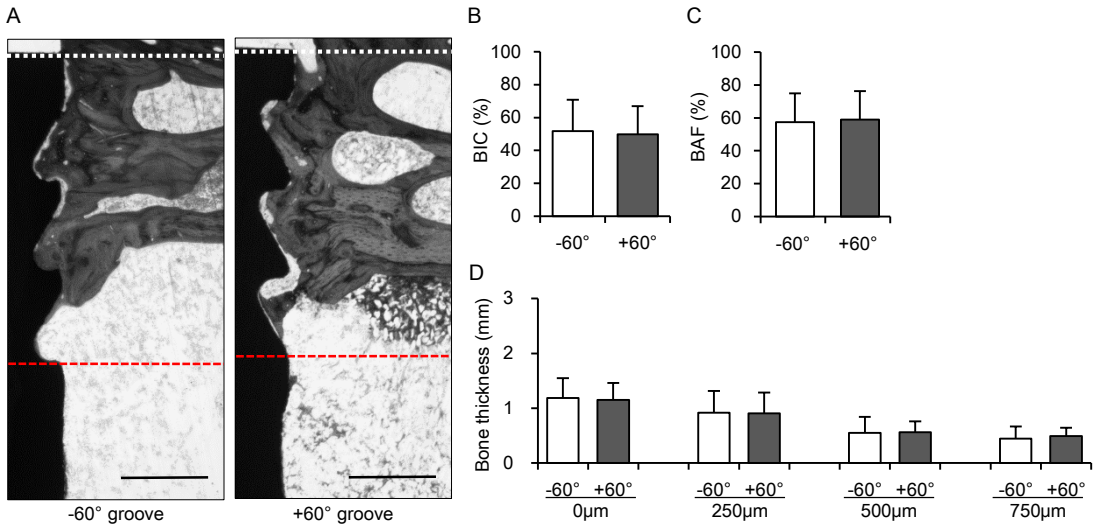
A
-60° groove
+60° groove
B
BIC (%)
100
80
60
40
20
0
-60°
+60°
C
BAF (%)
100
80
60
40
20
0
-60°
+60°
D
Bone thickness (mm)
3
2
1
0
-60° +60°
0μm
-60° +60°
250μm
-60° +60°
500μm
-60° +60°
750μm

Fig. 3

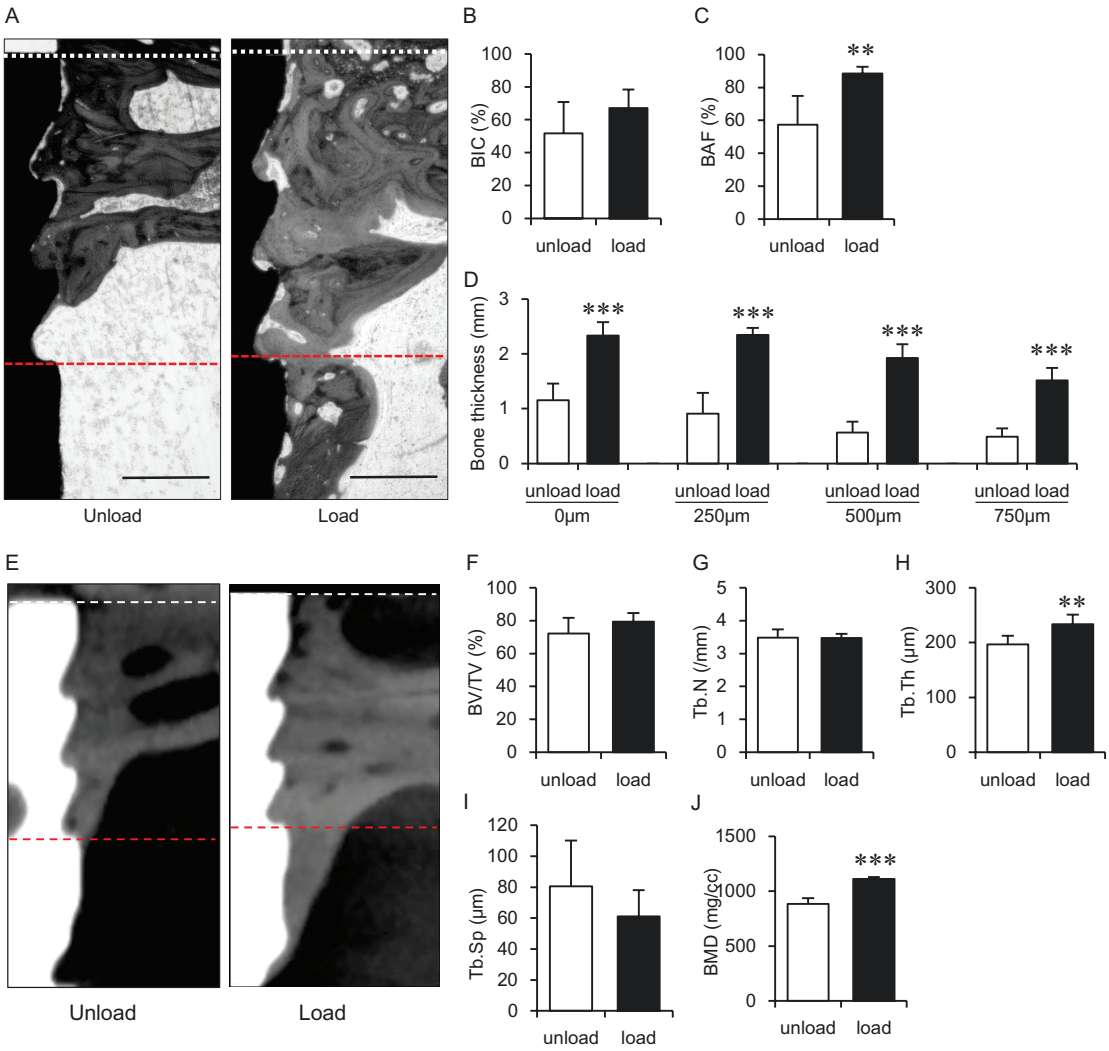
A
Unload
Load
B
BIC (%)
100
80
60
40
20
0
unload
load
C
BAF (%)
**
D
Bone thickness (mm)
***
unload load
0μm
250μm
500μm
750μm
E
Unload
Load
F
BV/TV (%)
G
Tb.N (/mm)
H
Tb.Th (μm)
I
Tb.Sp (μm)
J
BMD (mg/cc)
1500
1000
500

Fig.4

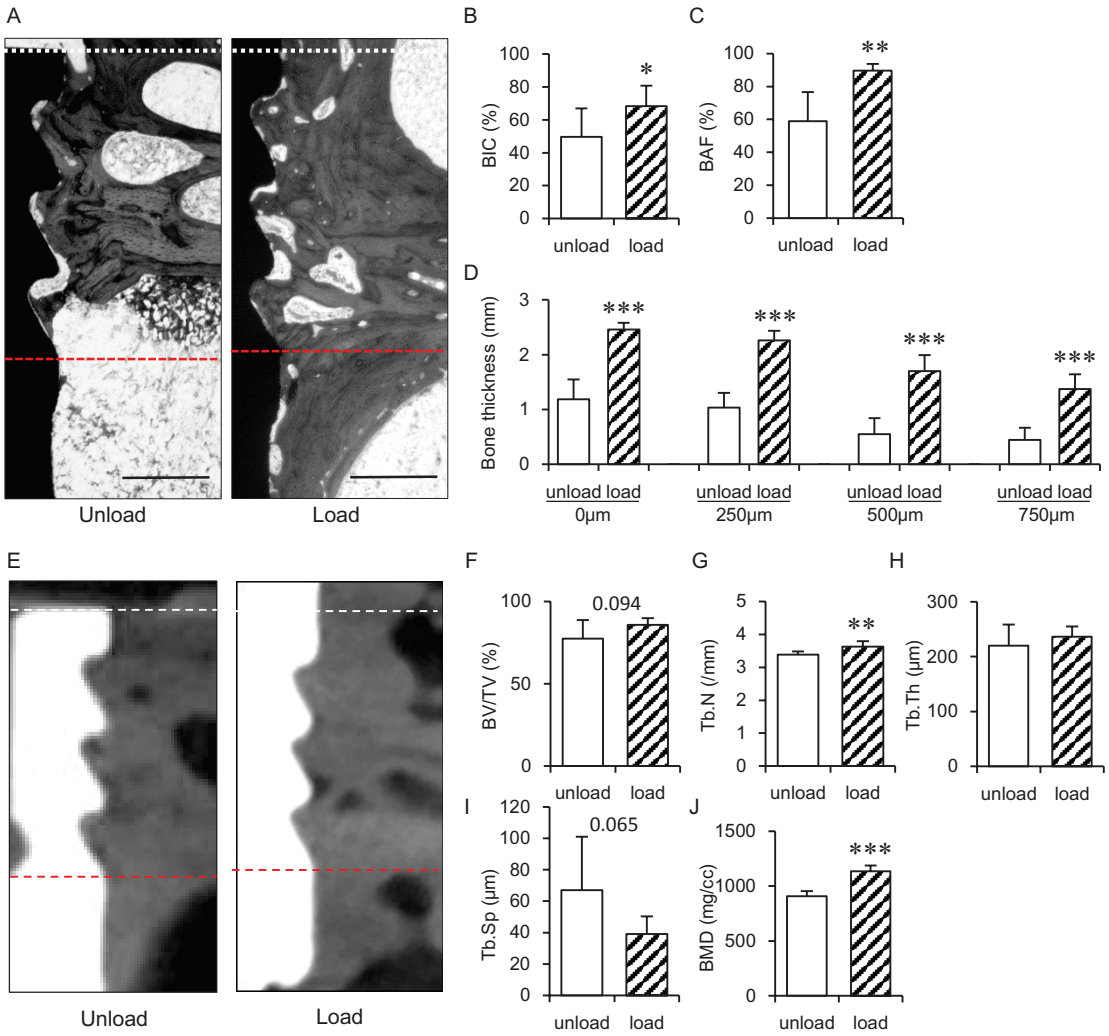
A
Unload
Load
B
BIC (%)
100
80
60
40
20
0
*
unload
load
C
BAF (%)
100
80
60
40
20
0
**
unload
load
D
Bone thickness (mm)
3
2
1
0
***
***
***
***
unload load
0μm
unload load
250μm
unload load
500μm
unload load
750μm
E
Unload
Load
F
BV/TV (%)
100
50
0
0.094
unload
load
G
Tb.N (/mm)
5
4
3
2
1
0
**
unload
load
H
Tb.Th (μm)
300
200
100
0
unload
load
I
Tb.Sp (μm)
120
100
80
60
40
20
0
0.065
unload
load
J
BMD (mg/cc)
1500
1000
500
0
***
unload
load

Fig.5

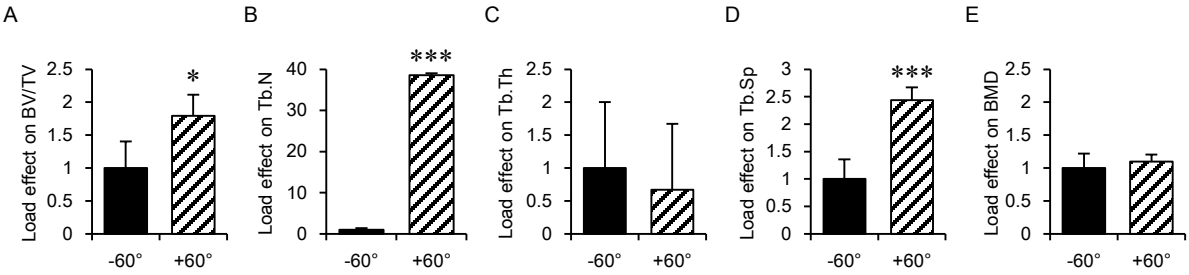
A
B
C
D
E
Load effect on BV/TV
Load effect on Tb.N
Load effect on Tb.Th
Load effect on Tb.Sp
Load effect on BMD
*
***
***
-60°
+60°